Regular Article – Experimental Physics

Interplay of the elastic and inelastic channels in the ^{16}O + ^{27}Al scattering at $E_{lab} = 280$ MeV

F. Cappuzzello[1,2], D. Nicolosi[1,2], R. Linares[3,a], J.R.B. Oliveira[4], J. Lubian[3], C. Agodi[2], D. Carbone[2], M. Cavallaro[2], P.N. de Faria[3], A. Foti[1,5], and M.R.D. Rodrigues[4]

[1] Dipartimento di Fisica e Astronomia Università di Catania, I-95125, Catania, Italy
[2] INFN, Laboratori Nazionali del Sud, I-95125, Catania, Italy
[3] Instituto de Física, Universidade Federal Fluminense, 24210-346, Niterói, RJ, Brazil
[4] Instituto de Física, Universidade de São Paulo, DFN, C.P. 66318, 05314-970, São Paulo, SP, Brazil
[5] INFN, Sezione di Catania, via S. Sofia, 64, I-95125, Catania, Italy

Abstract. Recent data indicated a nuclear rainbow-like pattern in the elastic scattering of ^{16}O + ^{27}Al at $E_{lab} = 100$ MeV that arises from couplings of the ground to the low-lying states of the ^{27}Al nucleus. Similar effect was identified in the elastic angular distribution of ^{16}O + ^{12}C at $E_{lab} = 281$ and 330 MeV. These experiments show a crucial role of microscopic details of nuclear structure in the elastic scattering of heavy ions at energies well above the Coulomb barrier. In this work we investigate the ^{16}O + ^{27}Al system at $E_{lab} = 280$ MeV for which a coupled channel calculation predicts a pronounced nuclear rainbow-like structure. Obtained experimental data show evidences of an important coupling of the elastic channel to the inelastic. Coupled channel calculations reproduce the experimental angular distributions when a re-normalization factor on the real part of the optical potential is introduced. A proper theoretical approach still requires a high degree of accuracy for the nuclear structure models and new tools to deal with collective excitations.

1 Introduction

Heavy-ion nuclear collisions are powerful tools to assess effective nuclear potentials. In such systems, the structure of the colliding particles plays a major role on the scattering observables. Specific information on nuclear structure can be extracted by studying direct reaction channels.

The elastic channel is the primary source of information of the nucleon-nucleon interaction in nuclear matter. For α-like systems, such as ^{16}O + ^{16}O at 350 MeV, the elastic angular distribution shows a Fraunhofer structure at forward angles and a nuclear rainbow with an Airy minimum at $\theta_{c.m.} \sim 43^o$ [1]. The appearance of a nuclear rainbow structure has been studied in many systems over a wide range of energies by means of the optical model formalism [2,3]. In other systems, like ^{16}O + ^{28}Si, an anomalously large cross-section at backward angles is observed in the elastic angular distribution [4,5]. In this case, global optical potentials in general describe very well the angular distributions at forward angles but fail to reproduce the gross structure and oscillations at backwards angles.

Modified optical potentials reproduce the large structure but within a restricted energy range. Later on, many interpretations were proposed like effects of cluster exchange, Regge poles and resonances but none of them consistently describe all data [5].

At energies around the Coulomb barrier few channels are acessible and the coupled channel (CC) formalism is useful to take them into account. At higher energies many channels are open-like multinucleon transfers, deep-inelastic collision and so on. In this case a complete microscopic description of the collision would require a too large model space to be implemented in calculations. In addition the connection between microscopic information and reaction channels is not straightforward.

A striking feature is that state-of-the-art CC calculations predict a new kind of rainbow-like structure [6]. For instance, recent experimental data for elastic and inelastic scattering of ^{16}O + ^{27}Al at 100 MeV [7] indicate a crucial role of the coupling of the ground to the low-lying collective states of ^{27}Al [8]. The observed rainbow-like pattern at large scattering angles rises from the couplings only [9]. Recent theoretical reanalysis of the rainbow scattering in the ^{16}O + ^{12,14}C systems also indicate a similar

effect at higher bombarding energy [10–12]. In the case of $^{16}O + ^{12}C$ the couplings of the ground state to the 2^+ and 3^- states of both projectile and target are necessary to reproduce a secondary rainbow-like pattern present at 281 and 330 MeV.

A comprehensive analysis of the role of couplings to inelastic channels on the elastic angular distributions for heavy systems demands understanding of the contribution of high-lying and collective states in scattering at energies well above the coulomb barrier. In this work we investigate the elastic and inelastic scattering of $^{16}O + ^{27}Al$ at 280 MeV (17.5 MeV/u). We choose this beam energy since a more pronounced rainbow-like structure due to the coupling of the elastic channel to inelastic channel was predicted [6]. At such high energy we can evaluate the approximate description of the low-lying excited state of ^{27}Al, that successfully reproduce the data at 100 MeV, and verify possible contribution of transfer couplings to the elastic channel. This work is organized as follows. In sect. 2 we give a brief description of the experimental setup and we present the collected data. Section 3 is devoted to the theoretical analysis. Finally, in sect. 4 we give our conclusions and remarks.

2 Experimental data

The experiment was carried out at the INFN-LNS using $^{16}O^{3+}$ beam at 280 MeV provided by the K800 Superconducting Cyclotron. An ^{27}Al self-suporting target of $109 \mu g/cm^2$ thickness was used. The scattered particles were momentum analyzed by the large acceptance magnetic spectrometer MAGNEX [13–15]. The horizontal and vertical angular acceptances of the spectrometer were between $-5.2°$ and $+6.3°$ and between $-7°$ to $+7°$ around the optical axis, respectively. Measurements were done at five different angular settings of the spectrometer optical axis ($10°$, $13°$, $18°$, $26°$ and $34°$) in the laboratory frame, covering a total angular range from $5°$ to $40°$ (corresponding to $8°$ and $58°$ in the centre-of-mass frame). The typical angular resolution was $0.3°$ (in the laboratory framework). At backward angles data were integrated over $1.0°$ due to low statistics. Further details on the data reduction for this system at high energy can be found in [16].

2.1 Excitation spectra

The ^{27}Al excitation energy spectra up to 40 MeV at two different forward scattering angular ranges is shown in fig. 1. These spectra show that the elastic peak is completely resolved from the inelastic peaks corresponding to the low-lying excited states of ^{27}Al (namely $1/2^+$ and $3/2^+$ at 0.84 and 1.01 MeV, respectively). The energy resolution is about 450 keV at forward angles, mainly due to beam emittance and the finite momentum and angular resolution of the spectrometer. At backward angles, kinematic broadening worsens the energy resolution to 650 keV. In such cases, a proper distinction between the elastic channel and the two first excited states of ^{27}Al was possible
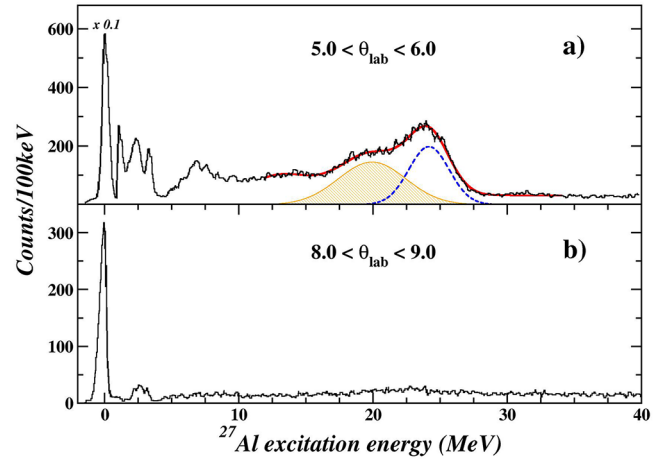
Fig. 1. (Color online) ^{27}Al excitation energy spectra at two different scattering angles: (a) $5° < \theta_{lab} < 6°$ and (b) $8° < \theta_{lab} < 9°$. The ^{27}Al ground-state peak is scaled by a factor 0.1 in (a). The broad structure between 13.0 and 30.0 MeV (panel a) is fitted by two Gaussian shapes (in orange hatched and blue dotted) on the top of a polynomial continuum.

by means of Gaussian shape fits to the peaks. Further details on the experimental setup and data reduction can be found in ref. [16].

The energy spectra show also a bell-shape–like envelope between 5.0 and 10.0 MeV due to the high density of excited states populated within this energy range. Similar structure was observed in (α, α') scattering, where the centroid energy of this group is about 8.5 MeV [17]. There are also two broad structures at higher excitation energies that are already suppressed at $9°$ scattering angle (see fig. 1(b)). This energy range is fitted by two Gaussian shape peaks on the top of a polynomial function. The latter effectively takes into account the continuum underneath the bumps due to ^{16}O particles originated from decay of ejectiles created in pick-up reactions like ^{17}O decaying into $^{16}O + n$. The centroid energies of the Gaussianlike structures are at ~ 20.0 and 24.1 MeV while the FWHM are ~ 6.0 and 3.6 MeV, respectively. The first one is interpreted as a Giant Quadrupole Resonance (GQR) mode of ^{27}Al, also observed in (α, α') experiments at approximately 18.5 MeV and $\Gamma \sim 7.6$ MeV, which are close to our observed values [17,18]. The second broad bump is a structure that is not observed in (α, α') experiments and a quantitative detailed analysis of this structure is beyond the scope of this work.

2.2 Angular distributions

Experimental elastic and inelastic angular distributions are presented in fig. 2. The inelastic data shown here correspond to the differential cross-section summed over the five low-lying states of ^{27}Al, namely $1/2^+$ at 0.84 MeV, $3/2^+$ at 1.01 MeV, $7/2^+$ at 2.21 MeV, $5/2^+$ at 2.73 MeV and $9/2^+$ at 3.00 MeV. Inelastic cross-sections are multiplied by a factor 100 for the sake of visualization of the experimental

data. The elastic channel is dominant at forward angle. The high-precision angular distributions allow one to draw some important model independent insights directly from the data. Firstly, elastic and inelastic angular distributions oscillate in opposition of phases at forward angles (see inset in fig. 2). According to Malfliet *et al.* [19] this behaviour appears whenever the elastic scattering is due to the nuclear ion-ion potential despite of other open channels at such high energy. Our second argument is based on the optical model. Considering the Sommerfeld parameter for $E_{lab} = 280 \, \text{MeV}$ ($\eta = 3.9$), a Fraunhofer-like behaviour is expected for the elastic distribution. Scattering cross-sections of this type are characterized by a Bessel function of the first order [20] which exhibits oscillations that roughly fall off exponentially. The experimental elastic distributions show oscillations with successive maxima (minima) separated by about $3°$ (see inset in fig. 2). Surprisingly two changes of slopes of the cross-sections are observed. Three orange dashed lines are superimposed to the angular distribution in fig. 2 to guide the eyes in order to highlight this feature. From them one observes changes of slope at $\sim 20°$ and $\sim 40°$ (indicated by vertical arrows) that may be related to the interference between the near/farside components. The first change of slope is located where a strong interference pattern is observed. This is the typical behaviour due to near/farside coherent scattering in the Fraunhofer regime. The second change seems to be related to a nuclear rainbow-like structure in the elastic scattering which is a genuine effect beyond the interpretation of the optical model in such strongly absorptive systems. In the next section we discuss this further in the light of coupled channel calculations.

3 Theoretical analysis

Our theoretical calculations follow the methodology indicated in refs. [6,8] and are summarized here. We use the code FRESCO [21]. The effective nucleus-nucleus potential consists of a Coulomb term and a complex nuclear potential given as follows:

$$U(r, E) = V(r, E)(N_r + iN_i), \quad (1)$$

where r is the relative distance of the colliding nuclei and E the centre-of-mass energy. $V(r, E)$ is the São Paulo potential in the local equivalent version $V(r, E) = V_{\text{folding}}(r)e^{-4(\frac{v(r)}{c})^2}$ where $v(r)$ is the relative velocity and $V_{\text{folding}}(r)$ is the double-folding potential [22]. The energy dependence of the potential is contained in the $e^{-4(\frac{v(r)}{c})^2}$ factor and arises from the Pauli non-locality.

The normalization factor for the real part (N_r) is set to 1.0 when couplings to the elastic channel are not strong. For weakly bound systems a reduction of the N_r down to about 0.6 is required to simulate the important coupling to the continuum in such cases [23,24]. The normalization factor for the imaginary part (N_i) is set to 0.6 in the entrance channel. This takes into account dissipative processes, like deep-inelastic collisions and transfer to the
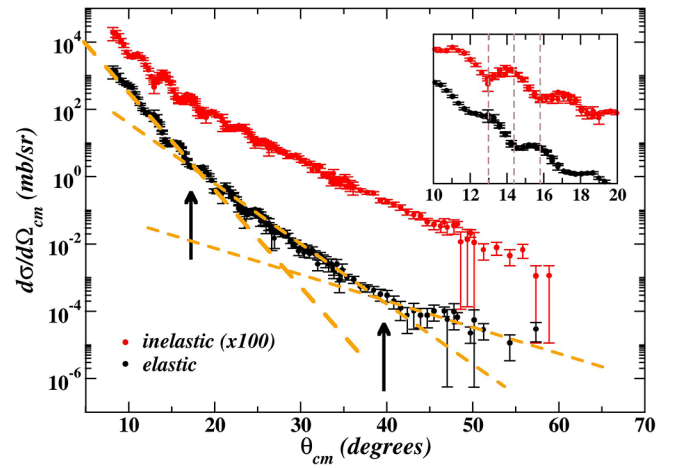
Fig. 2. (Color online) Angular distribution in the centre-of-mass frame for elastic (black) and inelastic (red) scattering of $^{16}\text{O} + ^{27}\text{Al}$ system at 280 MeV. Inelastic cross-sections are multiplied by a factor 100 for visual purposes only. The arrows indicate angles of deviation from exponentials fall off (orange dashed lines). The inset shows in detail the angular distributions at forwards angles (between $10°$ and $20°$).

continuum states [6] while other channels (inelastic and transfer) to bound states are explicitly considered in the CC scheme. To avoid double counting, a $N_i = 0.78$ is applied to the outgoing partition since this corresponds to the no coupling limit according to ref. [25].

The five low-lying states of ^{27}Al, $1/2^+$, $3/2^+$, $7/2^+$, $5/2^+$ and $9/2^+$ are effectively treated as a single state generated by a $1d_{5/2}$ proton hole coupled to the 2^+ rotational state of ^{28}Si core. For simplicity, herein they are referred to as the 2^+ state. Configuration mixing of the ^{27}Al $5/2^+$ ground state and the $5/2^+$ excited state (at 2.73 MeV) mainly results in a damping of the Fraunhofer oscillations, as demonstrated for a previous dataset at 100 MeV in ref. [26] and are not considered here. As already mentioned, this simple model successfully describes both elastic and inelastic experimental data of this system at 100 MeV [8,9]. Transfer processes can be a relevant mechanism at 280 MeV. Here we consider the $^{27}\text{Al}(^{16}\text{O}, ^{12}\text{C})^{31}\text{P}$ (α-transfer) and $^{27}\text{Al}(^{16}\text{O}, ^{15}\text{N})^{28}\text{Si}$ (p-transfer) since ^{12}C and ^{15}N ejectiles are clearly observed (see fig. 1a in ref. [16]).

3.1 The role of inelastic couplings

In fig. 3(a) the elastic experimental angular distribution is compared with calculations: Optical Model (OM), using the optical potential only (eq. (1)), and coupled channel (CC). The OM calculation does not agree with experimental data and does not indicate any rainbow-like pattern. In fig. 3(b) the inelastic angular distribution is also shown in comparison with calculations.

CC calculations were performed including the 2^+ and also adding the 4^+ and 6^+ low-lying states of ^{28}Si core. The quadrupole deformation parameters were taken
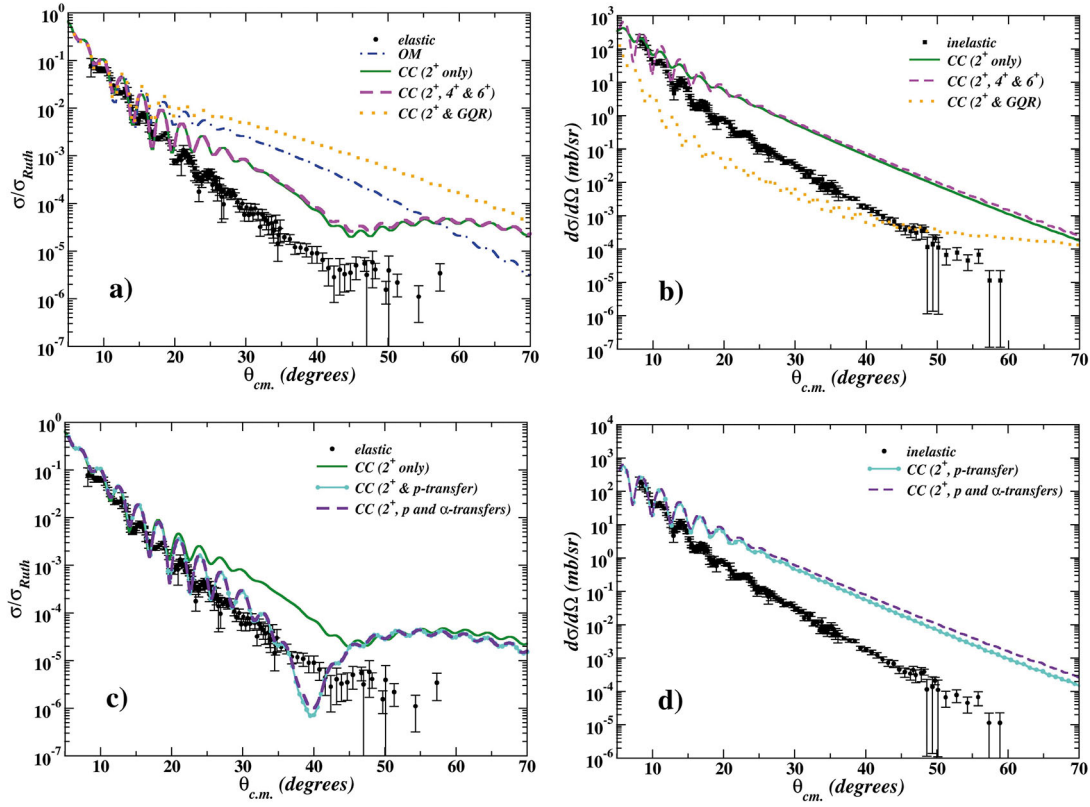
Fig. 3. (Color online) Comparison between calculations and experimental data at 280 MeV. The elastic (a) and inelastic (b) distributions are compared with the OM and CC calculations including coupling to excited states of ^{27}Al described as a $1d_{5/2}$ proton hole coupled to the 2^+, 4^+ and 6^+ rotational states of ^{28}Si core and to the GQR. In (c) and (d) the effects of the proton and α-transfer channels on the elastic and inelastic scattering are shown, respectively. See text for details.

from [27]. The relative importance of 4^+ and 6^+ to the elastic distribution is negligible compared to the CC coupled with the 2^+ only (see fig. 3(a)). For the present data local minima are reasonably well reproduced despite the differences in the amplitude of oscillations within the Fraunhofer diffraction region. Also the second change of the slope at about $40°$ is qualitatively reproduced. However the calculated cross-section at large angle is about one order of magnitude higher than the experimental data indicating that some aspect of reaction mechanism might still be missing. Calculations with model-independent deformed potentials, using experimental transition probabilities for the low-lying excited states of the ^{27}Al did not improve the agreement. We also considered the reorientation effect of the $5/2^+$ ground state and the configuration mixing in the $5/2^+$ ground state and $5/2^+$ excited state at 2.73 MeV. They both only contribute to smooth the oscillations in the elastic angular distribution and therefore are not shown here.

The GQR of ^{27}Al is a significant structure that appears in the energy spectra (see fig. 1) and, therefore, might be an important channel. Giant resonances are highly collective excitation modes characterized by oscillations of charge and mass that introduce difficulties in the nuclear reaction calculations. First, it is not clear that form factors, as considered for bound states, apply to the description of giant resonances as well. Secondly, the use of deformed potentials may not be appropriate. A more realistic approach would be to represent this structure as a set of representative states coupling with the elastic channel. In this case the calculations will strongly depend on the nuclear structures models for such set of states. A rigorous treatment of the GQR is beyond the scope of this work.

For a qualitative investigation of its influence on the elastic angular distribution, the GQR is treated as bound excited state centered at 20.0 MeV. Its strength was determined from scaling of the 2^+ ^{28}Si state following the energy weighted sum rule [28], from which we extracted an effective quadrupole deformation parameter $\beta_2 = 0.259$. According to our calculations, the coupling to the GQR worsen the agreement between the results of CC calculations and the data (fig. 3(a) dotted yellow line). Theoretical results for the cross-sections of the GQR structure shows an oscillatory behavior at forward angles followed by an exponential decay similar to the 2^+ angular distribution. This is expected since we are simulating this structure as a single bound state. Calculated cross-sections are of the same order of magnitude as the experimental one, as estimated from the energy spectra. However counting statistics do not allow for a proper subtraction of the continuum background and clear observation of an oscillatory structure in the angular distribution for the GQR. We also performed calculations with couplings of the ground to the the 3^- and 2^+ excited states of the projectile. These
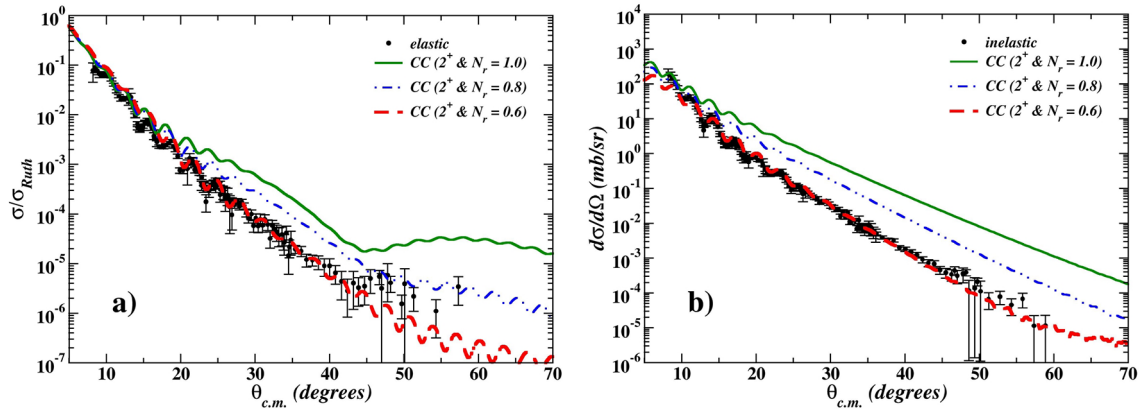
Fig. 4. (Color online) Elastic (a) and inelastic (b) calculations considering a re-normalization of the real part of the optical potential.

attemps did not improve the agreement with the experimental results and therefore are not shown here.

3.2 Effects of transfer couplings

Coupling effects due to particle transfer on the elastic and inelastic scattering were investigated as well. Coupled Reaction Channel (CRC) calculations were performed using the prior finite-range approximation, with full complex remnant and non-orthogonality corrections. In the coupling scheme we consider the p-transfer and α-transfer channels, always with only the 2^+ state of ^{28}Si core included. Spectroscopic amplitudes for p-transfer were taken from [29,30] where we included the bound states of ^{28}Si up to 4 MeV and the ground and the $5/2^+$ states of ^{15}N. In the case of α-transfer, we used the extreme cluster model. The relative motion of the alpha particle to the core is determined by the principal quantum number N and the orbital angular momentum L. In this case the intrinsic spin of transferred alpha particle is ($S = 0$) and its internal state is $1s$. In transforming the wave functions of the four independent nucleons (two protons and two neutrons) in orbits n_i, l_i into cluster, total number of quanta should be conserved according to the rule $\sum_{i=1}^{2} 2(n_i - 1) + l_i = 2(N-1) + L$ [31]. As in this case the four nucleons that are transferred are in the sd shell, independently in which single particle of state they are ($1d_{5/2}$, $2s_{1/2}$ or $1d_{3/2}$) the number of quanta per nucleon is 2. So, the total number of quanta is 8. This means that for $L = 0$, $N = 4$ and for $L = 2$, $N = 3$. These configurations account for the transfer to the g.s. and the lowest excited states of ^{31}P that are all positive parity. Only even values of L are allowed because the total number of quanta is even. Spectroscopic amplitude equal to 1.0, as it is usually assumed. The wave functions of the bound states of the proton or of the α-transfer were generated by a Woods-Saxon shaped potential, whose depth was adjusted to fit the experimental separation energies for proton and alpha particles. The reduced radii and diffuseness are 1.25 and 0.6 fm, respectively for both ^{16}O and ^{27}Al.

Results for elastic and inelastic scattering are shown in figs. 3(c) and 3(d), respectively. From fig. 3(c) one sees that the p-transfer channel produces a minimum around $\theta_{c.m.} \approx 40°$ but the shape of the elastic scattering angular distribution is not well reproduced. The α-transfer channel is found to give a negligible contribution. Therefore the inclusion of this transfer channel does not improve the agreement with experimental data. We also included additional bound states in the p-transfer coupling scheme with no revelant changes in the calculated cross-sections.

3.3 Re-normalization of the real part of the optical potential

Calculations shown so far achieved limited success in describing simultaneously the elastic and inelastic distributions. Possibly the couplings of the elastic channel to specific high-lying or continuum states may be very strong and are not properly treated in our calculations.

In nuclear reactions at high energies, the projectile-target distance is short and the densities overlap is large. States occupied in the target nucleus are forbidden for the nucleons of the projectile due to the Pauli principle. This effect lead to an effective transparency of nucleus-nucleus interaction. Very recently it has been shown that the three-nucleon-force [32] also suppress the interaction and may also be an important effect in our system.

Considering these arguments we performed CC calculations (including the 2^+ ^{28}Si core) with a re-normalization factor for the real part of the optical potential (eq. (1)). In fig. 4 we show the results for different values of N_r. The best overall agreement for both elastic and inelastic angular distributions over the entire angular range is found for $N_r = 0.6$ (see fig. 4(a) and (b), dashed red line). At forward angles it nicely reproduces oscillations observed on both experimental angular distributions. On the other hand, the calculation does not indicate the presence of an Airy-like minimum as it is suggested by the experimental data.

4 Conclusions

In this work we presented experimental data for the elastic and inelastic scattering for ^{16}O + ^{27}Al at 280 MeV

beam energy. The achieved energy resolution allowed a clear identification of the elastic peak. The experimental elastic angular distribution exhibits a rainbow-like pattern with a possibly Airy-like minimum around $40°$, where cross-sections are about 10^{-4} mb/sr. The calculation model, that successfully describes both elastic and inelastic dataset at 100 MeV, fails to precisely reproduce the dataset at 280 MeV. At such high energy a strength normalization factor of 0.6 in the real part of the potential is necessary to effectively account for the polarization due to the couplings to all missed channels. It must be emphasized that the calculation simultaneously describes experimental data for elastic and inelastic angular distributions in more than seven orders of magnitude. However, local minimum observed in the experimental data at $\sim 40^o$ is not well reproduced by this calculation.

The topic is still ambiguous and demands efforts on the microscopic description of the coupling due to high-lying excited states like the GQR. We see that the scattering of heavy ions far above the Coulomb barrier still retains information regarding specific details of internal degrees of freedom. Relevant effects at low cross-sections and high energies and the description of the scattering observables requires a high degree of accuracy of the nuclear structure. To overcome some of the difficulties connected to the structure of the odd deformed ^{27}Al nucleus a promising option is to study the elastic scattering of an even and spherical heavy nucleus probing cross-sections at the order of sub-μb/sr.

References

1. E. Stiliaris *et al.*, Phys. Lett. B **223**, 291 (1989).
2. M.S. Hussein, K.W. McVoy, Prog. Part. Nucl. Phys. **12**, 103 (1984).
3. D.T. Khoa, W. von Oertzen, H.G. Bohlen, S. Ohkubo, J. Phys. G: Nucl. Part. Phys. **34**, R111 (2007).
4. J.G. Cramer, R.M. de Vries, D.A. Goldberg, M.S. Zisman, C.F. Maguire, Phys. Rev. C **14**, 2158 (1976).
5. P. Braun-Munzinger, J. Barrette, Phys. Rep. **87**, 209 (1982).
6. D. Pereira, J. Lubian, J.R.B. Oliveira, D.P. de Souza, L.C. Chamon, Phys. Lett. B **670**, 330 (2009).
7. M. Cavallaro *et al.*, Nucl. Instrum. Methods A **648**, 46 (2011).
8. D. Pereira *et al.*, Phys. Lett. B **710**, 426 (2012).
9. J.R.B. Oliveira *et al.*, J. Phys. G **40**, 105101 (2013).
10. S. Ohkubo, Y. Hirabayashi, Phys. Rev. C **89**, 051601(R) (2014).
11. R.S. Mackintosh, Y. Hirabayashi, S. Ohkubo, Phys. Rev. C **91**, 024616 (2015).
12. S. Ohkubo, Y. Hirabayashi, Phys. Rev. C **92**, 024624 (2015).
13. A. Cunsolo *et al.*, Nucl. Instrum. Methods A **481**, 48 (2002).
14. A. Cunsolo *et al.*, Nucl. Instrum. Methods A **484**, 56 (2002).
15. F. Cappuzzello, M. Cavallaro, D. Carbone, A. Cunsolo, *MAGNEX: an innovative large acceptance magnetic spectrometer for nuclear reaction studies*, in *Magnets: Types, Uses and Safety*, edited by T. Akitsu (Nova Science Publishers, New York, 2012).
16. F. Cappuzzello *et al.*, Nucl. Instrum. Methods A **763**, 314 (2014).
17. C. Mayer-Böricke *et al.*, Nucl. Phys. A **293**, 189 (1977).
18. A. Kiss *et al.*, Phys. Rev. Lett. **37**, 1188 (1976).
19. R.A. Malfliet, S. Landowne, V. Rostokin, Phys. Lett. B **44**, 238 (1973).
20. P. Fröbich, R. Lipperheide, *Theory of Nuclear Reactions* (Oxford University Press Inc., New York, 1996).
21. I.J. Thompson, Comput. Phys. Rep. **7**, 167 (1988).
22. L.C. Chamon, D. Pereira, M.S. Hussein, M.A. Candido Ribeiro, D. Galetti, Phys. Rev. Lett. **79**, 5218 (1997).
23. Y. Sakuragi, M. Yahiro, M. Kamimura, Prog. Theor. Phys. **70**, 1047 (1983).
24. D.P. Souza *et al.*, Nucl. Phys. A **836**, 1 (2010).
25. L.R. Gasques *et al.*, Nucl. Phys. A **764**, 135 (2006).
26. F. Cappuzzello *et al.*, EPJ Web of Conferences **66**, 03067 (2014).
27. S. Raman, C.W. Nestor Jr., P. Tikkanen, At. Data Nucl. Data Tables **78**, 1 (2001).
28. A. Bohr, B.R. Mottelson, *Nuclear Structure*, Vol. **2** (World Scientific Publishing, Singapore, 1997).
29. M.A. Firestone *et al.*, Nucl. Phys. A **258**, 317 (1976).
30. B.H. Wildenthal, J.B. McGrory, Phys. Rev. C **7**, 714 (1973).
31. M. Moshinsky, Nucl. Phys. **13**, 104 (1959).
32. K. Minomo, M. Kohno, K. Ogata, Phys. Rev. C **93**, 014607 (2016).